V. Kratky
S. F. El-Hakim
Photogrammetric Research
National Research Council of Canada
Ottawa, Ontario K1A OR6, Canada

Quality Control for NRC On-Line Triangulation

The NRC ANAPLOT software is capable of interactive statistical testing for the presence and location of potential gross errors affecting the scale constrained orientation of consecutive models in bridging.

Abstract: *An efficient quality control of observed data by applying the data snooping technique for gross error detection has been implemented in the NRC ANAPLOT triangulation program. The exact values of the redundancy numbers are computed for each image point, a rigorous statistical test is applied, and the results are displayed. Weak points which are indicated by the test are remeasured, and the test is repeated before continuing with new photographs. Using different types of data, the ability of the technique to detect gross errors is studied and suitable point configurations are tested.*

Introduction

One of the most important applications of an on-line triangulation is a quality-controlled data acquisition followed by an off-line adjustment. One of the simplest ways of achieving this goal is to perform bridging in individual strips by consecutive relative orientation and scaling of models followed by a cross-tying of strips into a block (Kratky, 1980). After each orientation is carried out by the computer, y-parallaxes and tie discrepancies are computed and displayed for each point in the model. These parallaxes can indicate if a gross observational error or blunder has been committed. However, in many cases it is difficult, or even impossible, to locate correctly the point where the faulty observation took place. This is due to two reasons. The first is the low redundancy available in the model as a unit and the second is the high correlation between the residuals (or parallaxes) of some points. Therefore, relying on the magnitude of parallaxes for locating gross errors could be inefficient and misleading. The ability of the system to detect and locate gross errors improves by upgrading the geometry of intersecting rays and by using additional constraints. In addition, rigorous statistical testing, such as data snooping (Baarda, 1968) or "tau" criterion (Pope, 1976), can be applied.

The NRC on-line triangulation, developed for the ANAPLOT, employs a mathematical model for relative orientation with an additional scale transfer constraint and statistically tests the standardized residuals at measured image points. The full weight cofactor matrix of the residuals ($\mathbf{Q}_{vv}$) is computed for each point configuration used. From this matrix, points with highly correlated residuals can be identified. If these points have large residuals, the operator is able to identify the suspected point and reobserve only this point even though other points may display larger residuals.

The objective of this paper is to describe this aspect of the NRC on-line triangulation system. Using actual and simulated data, many of the factors affecting the ability of the technique to detect gross errors can be studied. Here, the effects of point configuration, density, and location are presented.

Basic Mathematical Model

In the ANAPLOT software the scale transfer from model to model in the process of bridging is determined simultaneously with the relative orien-

Photogrammetric Engineering and Remote Sensing,
Vol. 49, No. 6, June 1983, pp. 763-769.

0099-1112/83/4906-0763$02.25/0

tation of the model. In this instance the model coordinates of suitably chosen tie points in the preceding model directly constrain the intersections of corresponding rays in the new model.

Relative orientation of the first model is based on the determination of five unknown parameters whereas the simultaneous solution of the scaled orientation in subsequent models contains six unknowns. In order to preserve the uniformity of programming and an adequate real-time speed, the orientation of all models is formulated primarily with the use of the coplanarity condition. In addition, all models except the first one enforce the connection with preceding models by using a modified collinearity condition. The collinearity condition is applied only to tie points. Because the intersection with corresponding rays is already enforced by means of the coplanarity condition, which is very strong in the YZ plane, it is sufficient to check the ties with the previous model by specifying a single collinearity equation related to the XZ plane only.

Both conditions are applied in the following form:

$$\begin{aligned} &\bullet \text{ coplanarity} \quad F_p \equiv (\mathbf{b}\ \mathbf{x}'\ \mathbf{x}'') = 0, \\ &\bullet \text{ collinearity} \quad F_L \equiv \Delta X z'' - \Delta Z x'' = 0, \end{aligned} \tag{1}$$

where vector $\mathbf{b} = (1\ \beta_y \beta_z)^T$ represents the photogrammetric base normalized through its x-component into values $\beta_i = b_i/b_x$. Vectors $\mathbf{x}' = (x'\ y'\ z')^T$ and $\mathbf{x}'' = (x''\ y''\ z'')^T$ are derived by orthogonal transformation of the original camera coordinates using rotation matrices which are functions of the attitude elements κ, ϕ, ω. Values ΔX and ΔZ are model coordinates of tie points reduced with respect to the right projection center. All unknowns (β_x, β_y, β_z, κ, ϕ, ω) are dimensionless and expected to be of the same order of magnitude.

The computations are based on the combined form of least-square adjustment

$$\mathbf{Av} + \mathbf{Bg} + \mathbf{u} = 0 \tag{2}$$

converted into parametric form

$$\mathbf{Bg} = \overline{\mathbf{l}} + \overline{\mathbf{v}} \tag{3}$$

by interpreting the misclosure vector $\mathbf{u}$ as vector of pseudo observations $\overline{\mathbf{l}} = -\underline{\mathbf{u}} = -\mathbf{Al}$ with corresponding pseudo weights $\overline{\mathbf{P}} = (\mathbf{AQA}^T)^{-1}$ and pseudo corrections $\overline{\mathbf{v}} = -\mathbf{Av}$. Here, $\mathbf{A}$ and $\mathbf{B}$ represent the design matrices with respect to real observations x'', y'' and to unknown parameters $\mathbf{g}$, respectively, whereas $\mathbf{Q}$ is the weight cofactor matrix of observations $\mathbf{l}$.

Coordinates x'', y'' are the only observations in Equations 1 and are measured in a parallax mode with respect to fixed coordinates x', y', independently for each pair of rays. Consequently, matrices $\mathbf{A}_p$ and $\mathbf{A}_L$ have a diagonal form and their elements are

$$a_p = -z'_i, \quad a_L = -\Delta Z_i.$$

Recognizing the well known, experience-based relationship of *a priori* expected inaccuracies for x' and y' measurements

$$q_{yy} = 2q_{xx},$$

one defines

$$\mathbf{Q} = \mathbf{Q}_{xx} = \mathbf{I}, \quad \mathbf{Q}_{yy} = 2\mathbf{Q}_{xx} = 2\mathbf{I}$$

and derives

$$\overline{\mathbf{Q}}_{pp} = \mathbf{A}_p \mathbf{Q}_{yy} \mathbf{A}_p{}^T, \quad \overline{\mathbf{Q}}_{LL} = \mathbf{A}_L \mathbf{Q}_{xx} \mathbf{A}_L{}^T.$$

The pseudo weights to be associated with coplanarity and collinearity conditions treated simultaneously in a six parameter solution of Equation 3 are then

$$p_p = 1/2z_i'^2, \quad p_L = 1/\Delta Z_i^2. \tag{4}$$

Computation and Testing of Redundancy Numbers

The effect of a gross error Δl_i on the residual v_i of an observation l_i is

$$\Delta v_i = -r_i \Delta l_i \tag{5}$$

where r_i, called the redundancy number, is the i^{th} diagonal element of matrix $\mathbf{Q}_{vv}\mathbf{P}$. The weight cofactor matrix of the residuals, $\mathbf{Q}_{vv}$ is given by

$$\mathbf{Q}_{vv} = \mathbf{Q} - \mathbf{BN}^{-1}\mathbf{B}^T \tag{6}$$

where $\mathbf{N}$ is the normal equation matrix. The standardized residual w_i is computed by

$$w_i = v_i/\hat{\sigma}_{v_i} = v_i/(\hat{\sigma}_o\sqrt{q_i}) \tag{7}$$

where q_i is the i^{th} diagonal element of matrix $\mathbf{Q}_{vv}$.

Before trying to draw conclusions from the knowledge of redundancy numbers, it may be useful to demonstrate that they truly represent the actual situation. In other words, is Equation 5 valid for various practical cases? To answer this question numerous tests were conducted, in which gross error Δl_i was introducted to observation l_i and its effect Δv_i was computed after relative orientation and scaling. The expected $\Delta\overline{v}_i$ was also computed using Equation 5 and its values compared with the actual Δv_i. Different cases have been studied and some of the results are presented in Table 1. Point distribution is shown in Figure 1. Values of Δl_i are always equal to 100 μm. All the tests produced a complete agreement between the expected residual $\Delta\overline{v}_i$ and the actual residual Δv_i, demonstrating that the redundancy numbers, as computed by $\mathbf{Q}_{vv}\mathbf{P}$, are correct.

Table 2, based on real measurements, illustrates the distribution of an artificial error of 100 μm introduced in point 3, after orientation was completed (the point numbering as shown in Figure 1). The table also gives the y-parallax and

TABLE 1. TEST OF REDUNDANCY NUMBERS

Point #	Number of Points Used in Orientation	Faulty Coordinate	r_i	Expected $\Delta\bar{v}_i$ μm	Actual Δv_i μm
2	6	y'	0.75	75	76
2	9	y'	0.82	82	82
2	6	x'	0.00	0	0
2	6	x''	0.67	67	66
2	9	x''	0.67	67	66
2	6	y''	0.75	75	76
3	6	y'	0.09	9	10
3	9	y'	0.27	27	27
4	6	y'	0.28	28	28
4	9	y'	0.42	42	42
5	6	y'	0.35	35	35
5	9	y'	0.50	50	50

standardized residual for each of the six points. From the examination of y-parallaxes, point 2 seems to be the one in error, although this is not true. However, the largest standardized residual appears at point 3 where the error actually took place. It is obvious that the standardized residuals show the real significance of distributed discrepancies and that they should be tested for gross errors rather than the magnitude of parallaxes.

EFFECT OF POINT DISTRIBUTION AND DENSITY

When analyzing a suitable point distribution and density, two aspects of on-line triangulation must be considered—the accuracy of collected data and the efficiency of used procedures. The efficiency is not only judged by the time needed to perform the operations, but also by the intrinsic reliability of data. The on-line calculations are always applied to volume limited data and are not so much important for the final, usually independent, block adjustments as they are for the crucial function of quality control. One should take great care that statistical testing is not too adversely affected by the limited on-line geometry. The geometry will ultimately be improved in the final, simultaneous processing of data, but then statistical tests are much more difficult to run. It is important to consider suitable point configurations which guarantee high reliability of statistical testing rather than the highest possible accuracy of space limited photogrammetric solutions.

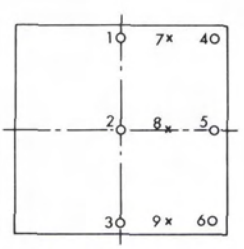

FIG. 1. Standard point distribution.

MODELS WITH NO SCALE TRANSFER

First models in every strip are computed only by relative orientation at a given scale. Because no scale transfer is applied, this computation is not typical for the on-line bridging process. Nevertheless, it is instructive to start our analysis with a model in which the coplanarity formulation is separated from other constraints.

It should be noted that the geometry of pure relative orientation is sensitive to relations governed by the y positions of corresponding points, with little or no respect to changes in x coordinates which primarily affect only the height definition of a measured point and not the orientation proper. Any statistical tests are, therefore, capable of detecting gross errors in y-coordinates, but even significant blunders in x may go undetected.

Figure 2 shows the redundancy numbers for measured y coordinates (or rather y-parallaxes) for points ranging from 6 to 15 in six different configurations (a) to (f). In general, the geometry of intersecting rays, which controls the success of relative orientation, is determined by the distribution of image points. A good geometry results in a high reliability of the orientation. The redundancy numbers, r, then indicate the local reliability of the adjustment as reflected by any particular observation. A low redundancy number reflects limited reliability, while its increased value means an improved reliability. For instance, the residuals at all corners of the six-point pattern (a) in Figure 2 will show only 8 percent of the actual local error.

The mechanism of the error distribution by Equation 5 is clearly illustrated by the full matrix $\mathbf{Q}_{vv}$. Figure 3 lists its values corresponding to

TABLE 2. DISTRIBUTION OF A GROSS ERROR IN PATTERN(a) IN FIGURE 4

Point #	1	2	3	4	5	6
Redundancy number r	0.09	0.77	0.07	0.32	0.40	0.23
y-parallax in μm	6.6	−20.7	6.6	−2.6	11.8	−2.0
Standardized residual w	1.38	1.44	1.51	0.27	1.14	0.25

the previous example. One should realize that the listed values are two times larger than the corresponding redundancy numbers, r. These are derived from the product $\mathbf{Q}_{vv}\mathbf{P}$ for which the weight matrix for y observations is, as shown above, $\mathbf{P}_{yy} = 0.5\mathbf{I}$. The six values in any i^{th} column of $\mathbf{Q}_{vv}$ express the proportional distribution of the error in the i^{th} observation over the six points used in the solution. Whenever an off-diagonal element exceeds or matches the diagonal one, the error distribution distorts the testing of errors by the magnitude of residuals, which becomes misleading and worthless. This is clearly documented in Figure 3 in each column of the matrix. All critical values are marked by boxes. The same effect is graphically represented in Figure 2 by heavy arrows indicating the direction of all critical, misleading transfers in pattern (a). The numbers at arrow lines are the critical weight cofactors from matrix $\mathbf{Q}_{vv}\mathbf{P}$, characterizing the degree of distortion. Also shown for each of the patterns in Figure 2 are the number of observations, n, and trace, tr, of the derived weight cofactor matrix $\mathbf{Q}_{gg}$ of unknowns, which could be used to assess and compare the expected accuracy of individual solutions.

The remaining sketches in Figure 2 can be analyzed in the same manner. The heavy arrows in patterns (b), (d), and (e) again indicate a critical transfer of errors. Dotted arrows in pattern (c) show an error transfer which is less critical, but still serious enough to be misleading. It is apparent that patterns (a), (b), (c), and (d) are very poor and, obviously, it is not only the number of points which improves the stability. The lowest redundancy numbers show in corners, and it appears to be very efficient to strengthen the stability by doubling points in critical areas, as shown in cases (e) and (f). These twin points will also show a high correlation between their r values; however, this is not critical any more. Because their location is almost identical, the problem area is uniquely identified. Also apparent from Figure 2 is the fact that the critical error transfers appear between neighboring points of low and high redundancy numbers, showing an imbalance in the error distribution. Ideally, one should strive for a balanced, uniform distribution of r values, however, still with a reasonable, not an excessively high, number of observed points. Because, by theory, the sum of r_i values is equal to the number of redundant ob-

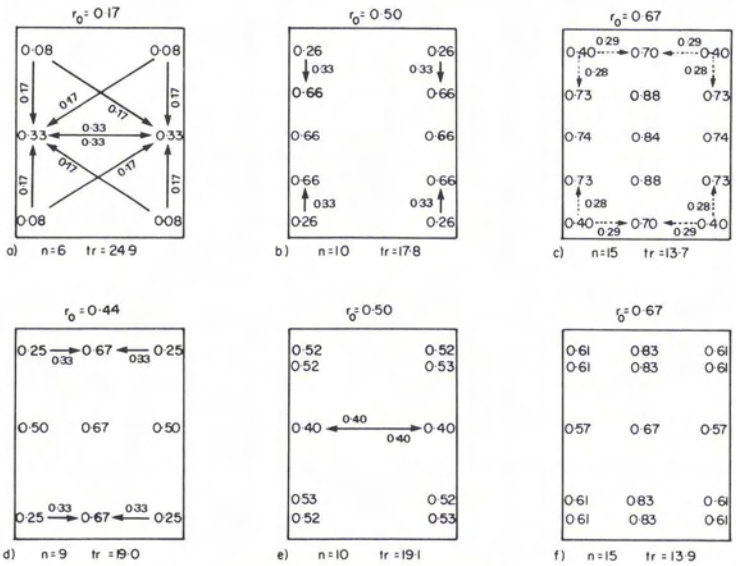

FIG. 2. Redundancy numbers for relative orientation without scale transfer.

0.17	-0.33	0.17	-0.17	0.33	-0.17
-0.33	0.67	-0.33	0.33	-0.67	0.33
0.17	-0.33	0.17	-0.17	0.33	-0.17
-0.17	0.33	-0.17	0.17	-0.33	0.17
0.33	-0.67	0.33	-0.33	0.67	-0.33
-0.17	0.33	-0.17	0.17	-0.33	0.17

FIG. 3. Matrix $\mathbf{Q}_{vv}$ for point pattern (a) in Figure 2.

servations in the system, the redundancy numbers average here at $r_o = (n - 5)/n = 1 - 5/n$. Pattern (f) is definitely the best configuration in Figure 2 as for the reliability of detecting gross errors and also rates well in the accuracy assessment. A very good distribution pattern, not shown in the figure, is achieved by measuring only 13 points (nine standard positions with four doubled corners). It yields r_i ranging from 0.58 to 0.80 with an average $r_o = 0.62$ and with the trace of $\mathbf{Q}_{gg}$ equal to 14.3.

MODELS WITH SCALE TRANSFER IN THREE TIE POINTS

The analysis of the scale constrained orientation of models can be conducted in a similar way, however, with taking into account the additional collinearity conditions. We will again consider a few standard point configurations and compare their reliability and accuracy potentials. The scale transfer is considered to be based on the use of three tie points distributed in the narrow overlap of three consecutive photographs.

Figure 4 illustrates a group of six different configuration patterns, each with three tie points and with the number of orientation points ranging from 6 to 13. The redundancy numbers are displayed separately for x'' observations at tie points and y'' observations at orientation points. Also listed for each pattern are the total number of observation points, the average redundancy number $r_o = (n - 3)/(n + 3)$, and the trace, tr, of the cofactor matrix $\mathbf{Q}_{gg}$.

We have demonstrated in the previous section that the standard six- and nine-point patterns are not suitable for on-line triangulation because of their critical error transfer, which prevents an efficient quality control. Nevertheless, they are included in Figure 4 as patterns (a) and (d) to allow for a comparison with corresponding patterns of Figure 2. The y-redundancy numbers are slightly increased and the critical transfers reduced due to the strengthening effect of scaling. The correlations among redundancy numbers within and between groups of observations x'' and y'' are demonstrated for the nine point pattern (d) by matrix $\mathbf{Q}_{vv}$ in Figure 5. The first three diagonal elements represent r values for observations x'', and the remaining diagonal elements are related to observations y'' in the sequence shown in Figure 1. The rest of the matrix shows correlations. For instance, there is no correlation between an x error in point 2 and y residuals for any other point.

The reliability of checking errors in y'' for patterns with 10 to 13 points in Figure 4 is generally good. However, it is obvious that three tie points do not support an adequate control of gross errors in the scale transfer. These poor conditions are practically uneffected by the number and configuration of other orientation points. The

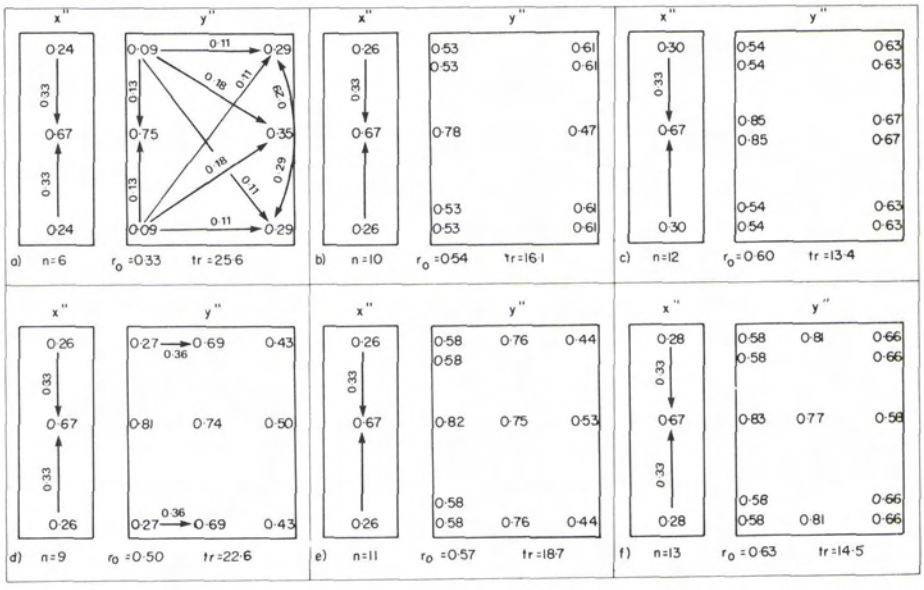

FIG. 4. Redundancy numbers for scale constrained relative orientation using three tie points.

0.26	-0.33	0.08	-0.06	-0.24	-0.06	0.18	0.00	0.18	0.06	-0.12	0.06
-0.33	0.67	-0.33	-0.00	-0.00	0.00	0.00	-0.00	-0.00	0.00	-0.00	0.00
0.08	-0.33	0.26	0.06	0.24	0.06	-0.18	0.00	-0.18	-0.06	0.12	-0.06
-0.06	-0.00	0.06	0.54	-0.18	0.21	0.05	0.33	-0.28	-0.71	0.08	-0.04
-0.24	-0.00	0.24	-0.18	1.63	-0.18	-0.14	-0.33	-0.14	-0.16	-0.35	-0.16
-0.06	0.00	0.06	0.21	-0.18	0.54	-0.28	0.33	0.05	-0.04	0.08	-0.71
0.18	0.00	-0.18	0.05	-0.14	-0.28	0.85	-0.33	0.52	-0.55	-0.24	0.12
0.00	-0.00	0.00	0.33	-0.33	0.33	-0.33	1.00	-0.33	-0.00	-0.67	0.00
0.18	-0.00	-0.18	-0.28	-0.14	0.05	0.52	-0.33	0.85	0.12	-0.23	-0.55
0.06	0.00	-0.06	-0.71	-0.16	-0.04	-0.55	-0.00	0.12	1.37	-0.08	0.04
-0.12	-0.00	0.12	0.08	-0.35	0.08	-0.24	-0.67	-0.23	-0.08	1.49	-0.08
0.06	0.00	-0.06	-0.04	-0.16	-0.71	0.12	0.00	-0.55	0.04	-0.08	1.37

FIG. 5. Matrix $\mathbf{Q}_{vv}$ for point pattern (d) of Figure 4.

shift of errors x'' from side points to the center, as documented numerically in the left upper 3 by 3 submatrix in Figure 5, remains critical in all patterns of Figure 4.

With reference to Figures 4(d) and 5, Figure 6 illustrates the effect of a gross error in a practical example of NRC ANAPLOT operations. The computer printout shows the way in which the statistical evaluation is displayed to the operator for his decision on which point should be remeasured.

```
 ID    PY     DX     DY     DZ
151    5.      0.     2.     1.
152   -6.      0.    -5.     1.
153   12.     -0.     5.    -2.
161   -5.
162    6.
163    2.                          Gross error of 50 µm in #153
154   -3.                          misleadingly shows largest
155    4.                          discrepancy at #156
156  -16.  <-------------------------------------------------

 ID  RED-N  PARX  EXPD   SIGF     SNOOPING STATISTICS
151   0.25  -0.9   3.4   0.27
152   0.67  -0.3   5.5   0.06
153   0.26   1.2   3.4   0.36

151   0.27   5.4   5.0   1.09                Statistically
152   0.81  -6.1   8.7   0.71                most likely
153   0.27  12.1   5.0   2.42  <-------------error location
161   0.43  -4.9   6.3   0.78
162   0.50   6.0   6.8   0.88
163   0.43   1.5   6.3   0.24
154   0.69  -2.7   7.9   0.34
155   0.75   4.4   8.3   0.54
156   0.69 -15.7   7.9   1.98

STANDARD ERROR OF UNIT WEIGHT =  6.8 MICRONS

MORE POINTS?

ANY REJECTION? ENTER ID!   153

REPLACEMENT? Y

  153   3     3.

 ID    PY     DX     DY     DZ
151   -1.     -0.     0.    -1.          Discrepancies after
152   -1.      0.    -2.     0.          correcting #153
153   -6.      0.    -2.     1.
161    5.
162   -5.
163    0.
154   -1.
155    2.
156    7.

STANDARD ERROR OF UNIT WEIGHT =  3.4 MICRONS
```

FIG. 6. Example of ANAPLOT data snooping.

Parallaxes and tie discrepancies are followed by a table which lists, for each measurement, the corresponding redundancy number (RED-N), x- or y-parallaxes both computed (PARX) and statistically expected (EXPD), as well as the error significance (SIGF) represented by the standardized residual. Otherwise, Figure 6 is self-explanatory.

MODELS WITH SCALE TRANSFER IN FIVE TIE POINTS

It is logical to expect an improvement in the scale transfer reliability by increasing the number of the points, from three to five, but not necessarily raising the total number of observations in the model. The number of 10 to 15 points has already proved to be useful. If the distribution of existing tie points on the left side of the model is mirrored on the right side for future tie points in the next model, one can choose one of the patterns described in Figure 7. Values r are graphically distributed in the same format as in previous figures and complemented by information on n, r_o, and tr. Pattern (a) with a regular distribution of ten points again displays weak upper and lower sides with a critical or serious transfer for three pairs of points. An alternate selection of double points in weak model parts works very well and all other patterns in Figure 7 guarantee a good quality control. Variant (c) with 13 points represents an excellent practical choice. It almost matches the accuracy and reliability of the 15-point pattern while surpassing it in efficiency due to the lower number of observations.

CONCLUSIONS

The NRC ANAPLOT software for on-line triangulation is capable of interactive statistical testing for the presence and location of potential gross errors affecting the scale constrained orientation of consecutive models in bridging. Based on numerous on-line simulations and practical experiments, a standard configuration of 13 orientation points including 5 tie points is considered best for a practical routine use.

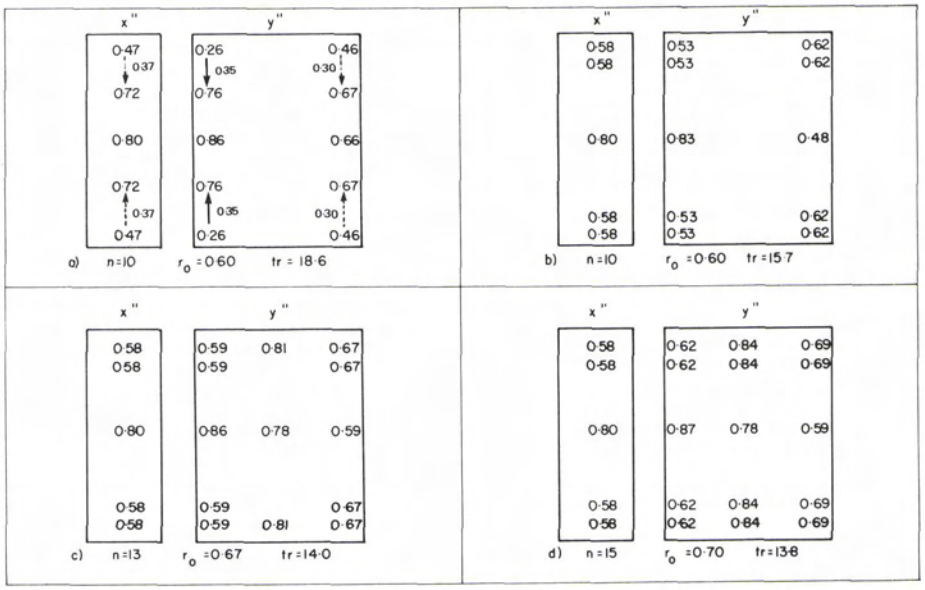

FIG. 7. Redundancy numbers for scale constrained relative orientation using five tie points.

REFERENCES

Baarda, W., 1968. *A Testing Procedure for Use in Geodetic Networks*, Netherlands Geodetic Commission, New Series, Vol. 2, No. 5, Delft, 97 p.

El-Hakim, S. F., 1981. A Practical Study of Gross-Error Detection in Bundle Adjustment, *Canadian Surveyor*, 35(4): 373-386.

Kratky, V., 1980. On-Line Aerial Triangulation on the ANAPLOT, *Proceedings of the ASP Analytical Plotter Symposium*, Reston, pp. 207-224.

Pope, A. J., 1976. *The Statistics of Residuals and the Detection of Outliers*, NOAA Technical Report NOS 65 NGS 1, Rockville, 133 p.

(Received 29 October 1982; accepted 17 February 1983)

Forthcoming Articles

G. E. Bormann and *E. Vozikis*, Map Projection Transformation with Digitally Controlled Differential Rectifiers.

James R. Carr, *Charles E. Glass*, and *Robert A. Schowengerdt*, Signature Extension Versus Retraining for Multispectral Classification of Surface Mines in Arid Regions.

B. E. Frazier and *G. K. Hooper*, Use of a Chromogenic Film for Aerial Photography of Erozion Features.

Klaus Hildebrand, New Generation Lens Systems for the Wild Aviophot Aerial Camera System.

John R. Jensen, Educational Image Processing: An Overview.

Ralph W. Kiefer and *Fred J. Gunther*, Digital Image Processing Using the Apple II Microcomputer.

T. H. Lee Williams, *Christopher Gunn*, and *Jeffrey Siebert*, Instructional Use of a Mainframe Interactive Image Analysis System.

J. Ronald Eyton, A Hybrid Image Classification Instructional Package.

Eric S. Kasischke, *Robert A. Shuchman*, *David R. Lyzenga*, and *Guy A. Meadows*, Detection of Bottom Features on Seasat Synthetic Aperture Radar Imagery.

Thomas R. Loveland and *Gary E. Johnson*, The Role of Remotely Sensed and Other Spatial Data for Predictive Modeling: The Umatilla, Oregon, Example.

Ross F. Nelson, Detecting Forest Canopy Change Due to Insect Activity Using Landsat MSS.

Albert L. Zobrist, *Nevin A. Bryant*, and *Ronald G. McLeod*, Technology for Large Digital Mosaics of Landsat Data.